A good-practices guideline for 6-DoF IMU-based dead-reckoning

James Schipmann Eger[1], Mauricio de Campos Porath[1], and Gustavo Daniel Donatelli[2]

[1] Federal University of Santa Catarina, Laboratory of Industrial Geodesy, Joinville SC, Brazil
james.eger@ufsc.br,
WWW home page: lgi.ufsc.br

[2] Federal University of Santa Catarina, Reference Centers in Innovative Technologies, Florianopolis SC, Brazil

Abstract. Position and orientation of an IMU can be obtained by the process known as dead-reckoning, which consists of mathematical operations on the measured inertial data. Ideally, this process would provide exact results. In practice, difficulties arise from a great number of variables involved. As can be assessed from literature review, lots of efforts have been made to deal with this complex problem; on the other hand, a more holistic and didactic approach is rare to be found. This work proposes an organized overview of the error sources affecting the measurement result, as well as the clarification of some relevant terms. Additionally, a dead-reckoning algorithm is presented, including a minimal data-processing package that has shown to bring significant benefits to the performance while keeping a more generalist character. We believe that these contributions lay useful foundations for further studies on the matter.

Keywords: MEMS, IMU, dead-reckoning, pose.

1 Introduction

Microelectromechanical systems (MEMS) own attractive characteristics such as: low size and weight (therefore portability), affordable cost and no need for a line-of-sight between the sensor and the object under measurement. Owing to these characteristics, MEMS-type inertial sensors have become ubiquitous in many fields of applications, including localization (indoor- and outdoor positioning), navigation, health care and sports (motion tracking of humans), consumer electronic products (e.g. tablets and smartphones), among others [24, 13].

A set of inertial sensors in a unit is called an inertial measurement unit (IMU). A six-degree-of-freedom IMU comprises a triad of mutually orthogonal accelerometers and a triad of mutually orthogonal gyroscopes, both triads sharing the same origin; additional sensors and other electronics are commonly included [1].

Position and orientation of an IMU can be obtained by the process known as dead-reckoning (DR): mathematical operations on the measured inertial data (i.e. linear accelerations and angular velocities) yield changes in orientation and position of the sensor. Ideally, the dead-reckoning process would provide exact results; in practice, difficulties arise from limitations of the sensors, data-processing steps and also from experimental scenario [5, 6, 20, 31, 13]. Although noise is known to be the most critical problem inherent to IMUs, the exact mechanism with which it is reflected on the accuracy of calculated pose is still not completely clear due to the number of variables involved.

Dead-reckoning utilizing MEMS-type IMUs is of high interest to the industrial and academic communities. For example, [25] developed a system based on a multi-sensor platform for reconstructing motorcycle trajectories; [16] proposed an instrument for surveying underground pipelines; [23] explored the credibility of using MEMS-IMUs for complementing existing systems on board Dynamic Positioning Vessels; [33] described a kalman filter-based framework to estimate pose and traveling speed of a welding torch; [34, 30] proposed solutions for *pedestrian dead-reckoning* problems; recent research advances make use of deep learning for performing IMU-based dead-reckoning [6, 12, 4, 17]. As can be assessed from the literature review, lots of efforts have been made to deal with this complex problem in many contexts; on the other hand, a more holistic and didactic approach is rare to be found. This work intends to share an approach to the problem of measuring the pose of six-degree-of-freedom MEMS-IMUs using the dead-reckoning principle. These findings result from deep literature review as well as from experience gained from experimentation with real data. Contributions include a comprehensive overview of the main factors affecting the measurement and a stepwise data-processing implementation.

Section 2 presents an organized overview of the sources of error that affect the measurement results; section 3 presents the proposed data processing steps; in section 4 two application examples using real experimental data are presented, followed by the conclusions in section 5.

2 Summary of errors sources

For the purpose of organization, we classify the main error sources into two categories: error sources *inherent to the sensor*; and those related to the *measurement task and data acquisition and processing.* We remark that this is not an exhaustive list of the error sources, but of the most relevant ones.

Error sources inherent to the sensor

Scale factor is the relation between input signal variations and output signal variations; Scale factor error is the deviation of the input-output gradient from unit; Scale factor repeatability refers to changes in scale factor that occur between periods of operation.

ORTHOGONALITY errors occurs when any of the axes of the sensor triad deviates from mutual orthogonality. It implies cross-coupling effects

DRIFT results from the integration of an uncompensated bias. An accelerometer bias will introduce an error proportional to time t in the calculated velocity and an error proportional to t^2 in the position due to the integration of the signal. Similarly, in the case of gyroscopes, an uncompensated bias will introduce an error proportional to t in the calculated angle [1]. This time-growing error can be called a *drift due to bias*, i.e. the result of integrating an uncompensated bias in the sensor output.

Bias in MEMS might vary slowly with time within a run, which is called BIAS INSTABILITY, defined by the standard [10] for both accelerometer and gyroscope as "the random variation in bias as computed over specified finite sample time and averaging time intervals. This non-stationary process is characterized by a $1/f$ power spectral density". In other words, in MEMS sensors, the bias wanders over time as a result of flicker noise.

Bias might also vary between runs (from turn-on to turn-on). This is represented by the BIAS REPEATABILITY, which quantifies the changes in bias that occur between specified periods of operation [9].

RANDOM WALK can be explained as follows: using the rectangular rule, numerical integration of sampled white noise is mathematically expressed by equation 1 [11]:

$$x_{k+1} = x_k + w_k \cdot \delta t \tag{1}$$

where: x_k represents the value of the random walk at time instant k; w_k is the sampled white noise; δt is the sampling interval (inverse of acquisition frequency, f_s).

White noise in MEMS is properly modeled as a normal random variable distributed as $w_k \sim N(0, \sigma^2)$ [11]. For an integration time $t = n\,\delta t$, the resulting random walk, i.e. the cumulative sum of sampled white noise, is a random variable with zero mean and variance which grows proportionally to integration time t (equation 2):

$$\begin{aligned} V(\sum^n x_k) &= V(\sum^n w_k\,\delta t) \\ &= (\delta t)^2 \cdot V(w_1 + w_2 + \cdots + w_n) \\ &= (\delta t)^2 \cdot n \cdot \sigma^2 = (\delta t)^2 \cdot \frac{t}{\delta t} \cdot \sigma^2 \\ &= \delta t \cdot t \cdot \sigma^2 \end{aligned} \tag{2}$$

In the case of gyroscopes, integration of white noise causes a first-order random walk known as *angle random walk*; similarly, in the case of accelerometers, it causes a first-order random walk in velocity known as *velocity random walk*, and a second-order random walk[3] in position.

[3] The result of integration of a first-order RW.

Error sources related to the measurement task and data acquisition and processing

In addition to those related to the sensor, other aspects will influence the error in position obtained by dead-reckoning of inertial measurements, as has been pointed out in the works from [27, 15, 5, 20, 28, 2]. We divide these aspects in two groups: aspects related to the *measurement task* and those related to *data acquisition and processing*.

The former group includes complexity and experimental conditions of each measurement task such as: motion intensity (fast or slow translations or rotations); existence of vibrations or jerky motions; duration of measurement.

The latter includes: sampling frequency; sensor fusion algorithm (orientation algorithm); numerical integration scheme (rectangular rule, trapezoidal rule, etc.); various other data processing techniques such as high/low-pass filters, motion detection, bias compensation, *et cetera*.

It is important to stress that there might be interaction between the aforementioned factors. Given the complexity of this scenario, an exhaustive analysis of the influence of each factor is virtually impossible. The goal of this summary is to provide an organized overview of the main aspects affecting the error in position. This overview is illustrated in Figure 1.

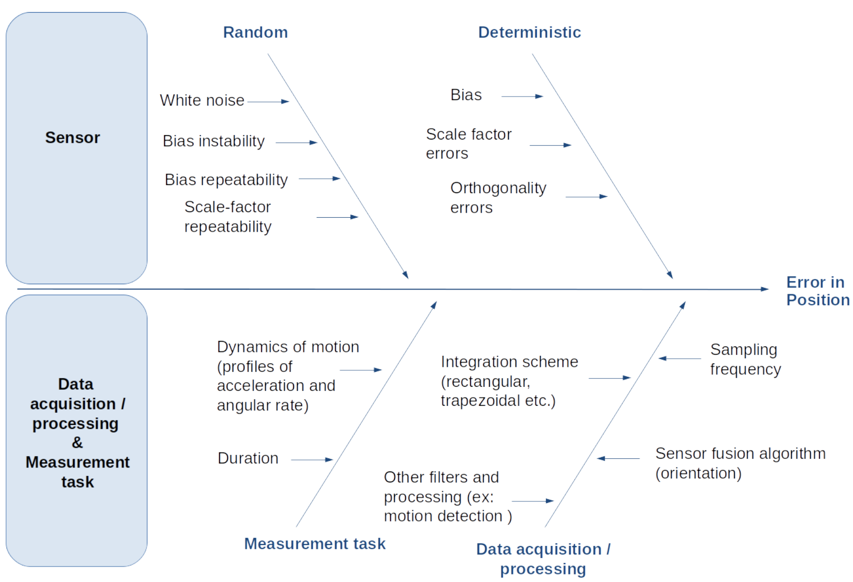

Fig. 1: Main sources of error in position measured by dead-reckoning with MEMS-type IMUs.

3 Dead-reckoning algorithm

The dead-reckoning algorithm implemented in this work consists of two blocks: first, orientation is obtained by an adaptation (slightly modified) of a well-known open-source algorithm from [18], the "Madgwick Algorithm"; then accelerations are double integrated using rectangular rule to yield position.

Characteristics such as low computational cost, good levels of accuracy and easy tuning have made the Madgwick Algorithm widely acknowledged "as having had a disruptive impact in inertial measurements" [29] — indeed, it is commonly used as a benchmark when evaluating other SFAs [19]. The algorithm employs a quaternion representation of orientation to describe the coupled nature of orientations in three-dimensions and is not subject to the problematic singularities associated with an Euler-angle representation. A constant-gain filter - called Gradient Descent Algorithm - is adopted to estimate the attitude of a rigid body in quaternion form by using data from a IMU (or MARG) sensor: a first quaternion estimation is obtained by gyroscope output integration and then it is corrected by a quaternion from the accelerometer (and magnetometer) data computed through a gradient descent algorithm. The fusion process is governed by a unique parameter (β). The choice of β depends on the magnitude of error expected due to integration of gyroscopes' noise. It can be defined according to equation 3 [18, 14]:

$$\beta = \sqrt{\frac{3}{4}} \cdot \sigma_\omega \tag{3}$$

where σ_ω is the standard-deviation of white noise in the gyroscopes.

A low value of β gives more weight to the gyroscope measurements; in turn, a high β gives more weight to accelerometers (magnetometers) measurements. The combination of sensors allows the gyroscope to track orientation during high frequency motion while gyroscopic drift is compensated during low frequency motion using the gradient descent steps.

Additional processing techniques

In order to provide meaningful DR results, some additional signal processing techniques were included, intending to be up-to-date with the state-of-the-art, as simple and generic as possible and without artificial manipulation of the measured data. The techniques are:

- Integration of signal is carried out only when the IMU is submitted to acceleration due to motion;
- Residual (fixed) bias is estimated and compensated;
- White noise is filtered by means of a wavelet filter;
- Adaptive gain for the sensor-fusion algorithm.

Integrate only during motion periods:

Since the integration of measurement errors such as noise and uncorrected biases causes the error in dead-reckoning to rapidly accumulate with time, it does make sense to perform integration only when there is motion of the IMU. Thus, a strategy to identify motion and stationary periods is applied in order to avoid unnecessary error accumulation.

We implemented a strategy that is grounded in the work from [21]. It is based on the variance of the magnitude of acceleration. First, magnitude of acceleration is calculated for each time stamp i as in equation 4:

$$f_{mag,i} = \sqrt{f_{x,i}^2 + f_{y,i}^2 + f_{z,i}^2} \quad i = 1, ..., N. \tag{4}$$

where: $f_{x,i}, f_{y,i}, f_{z,i}$ are the outputs from the accelerometers triad for x, y and z axis, respectively; N is the total number of measurements.

Then, the variance of magnitude is obtained 5:

$$\hat{V}_{f_{mag,j}} = \frac{1}{n-1} \sum_{j=n+1}^{N-n} (f_{mag,j} - \bar{f}_{mag,j})^2 \tag{5}$$

where: $\hat{V}_{f_{mag,j}}$ is the variance of the magnitude of acceleration for each sample j; n is the sample size for variance calculation; $\bar{f}_{mag,k}$ is the magnitude average of each sample.

The moments corresponding to motion are determined by comparing $\hat{V}_{f_{mag,j}}$ with a threshold, which is defined by trial-and-error. We use the average of initial stationary data (few seconds) as a basis for defining the threshold in this trial-and-error process.

Bias estimation and compensation:

At this point, it has become evident the importance of estimating and compensating biases in the MEMS sensors' outputs. In the case of gyroscopes, it can be done by simply averaging a set of measurements while the sensor is at rest; in the case of accelerometers, it is not so straightforward, since they sense acceleration due to gravity all the time.

For that matter, this work has implemented the method proposed by [26], which is based on a multi-position scheme: for the accelerometer triad, the total specific force measured in any orientation of a stationary IMU should be equal to the magnitude of local gravity. The IMU is then moved to a set of different and temporarily static orientations. From this, the following cost function $G(X)$ is derived (equation 6):

$$G(X) = \sum_{k=1}^{N} \left(\|h(\mathbf{f_{m,AV}}, \mathbf{X})\|^2 - \|\mathbf{g}\|^2 \right)^2 \tag{6}$$

Where: N is the number of different orientations (static intervals); $\mathbf{f_{m,AV}}$ is the average of measured specific force during each static interval; $\mathbf{X}$ is a vector containing bias terms (and other parameters) to be found; $\|\mathbf{g}\|$ is the magnitude of the local gravity vector.

The bias terms and other unknown parameters are found by minimizing the cost function $G(X)$.

White noise filtering:

White noise is one of the main issues that affect the performance of IMUs. *Wavelet filters* are well-suited for filtering this kind of noise, as has been shown in the works from [25], [8], [22] and [3]. Its main advantageous characteristics are:

- Ability of denoising a signal without appreciable degradation of the original signal
- Ability of denoising complex signals far better than conventional filters that are based on the Fourier transform;
- Efficiency in removing noise where the noise and signal spectra overlap;
- Little or no phase shifting of the original signal.

A wavelet is a wave-like function with an amplitude that starts and ends at zero, which is used to transform the signal to the wavelet domain. It acts as a window function that moves forward in time. The chosen wavelet is called *wavelet mother*, and there are infinite choices for it. Examples of typical ones are: Daubechies, Meyer and Coiflet. The main idea behind the wavelet filter is decomposing a signal into different scales which can be considered as frequency bands [7]. This decomposition is done by a set of consecutive low- and high-pass filters, which are determined by the wavelet mother.

Intending to reduce the effects of the white noise present in the IMU's outputs, we include a wavelet filter processing on the whole set of measured data before performing the dead-reckoning.

Adaptive gain for the SFA:

The SFA used in this work (Madgwick Algorithm) has one adjustable filter parameter, β, whose function is to give more or less weight to gyroscopes' measurements in the fusion process. Depending on the dynamics of measurement task, data from different sensors may be more or less reliable. Thus, instead of using a unique constant value of β for the whole dataset, it is beneficial to adaptively set its value, according to the dynamics of the motion [32, 20, 5].

We implemented a strategy based on the work from [32]. Switching logics are based on system dynamics sensed by the accelerometers to yield improved performance of the SFA. In brief, the scalar dynamic acceleration, α_{acc}, is defined as in equation 7:

$$\alpha_{acc} = \left| \frac{\|\boldsymbol{f}\| - \|\boldsymbol{g}\|}{\|\boldsymbol{g}\|} \right| \tag{7}$$

where: α_{acc} is the scalar dynamic acceleration, in units of g; $\|\boldsymbol{f}\|$ is the norm of the specific force vector (accelerometers measurements) and $\|\boldsymbol{g}\|$ is the magnitude of local gravity.

Distinction between low and high dynamics is done by comparing α_{acc} with a threshold, $\alpha_{threshold}$, which is determined empirically.

If the IMU is under high dynamics, accelerometers become less reliable for the orientation calculation, so a lower value of β should be used. Since we chose an IMU implementation (i.e. no magnetometers), we give full weight to gyroscopes in this circumstance. The implemented switching-logic is:

- If $\alpha_{acc} > \alpha_{threshold}$, $\beta = 0$;
- Else, β holds its predetermined value.

4 Experimental Results

We present two application examples of the proposed approach. First one consists of an original experiment and the second uses data from the dataset published by [15]. All algorithms have been developed in the *GNU Octave* programming language.

4.1 Application Example 1

The IMU is a XSens-MTi-G-700. Data acquisition was made by means of the XSens MT Manager software and a personal computer.

A Romi D-600 CNC machining center has been used to move the IMU and also for providing ground truth values of position. Sub-millimiter positioning errors are expected for this machine, which makes it a suitable reference system for this application, since the expected errors of this dead-reckoning process are, optimistically, in the order of a few millimeters.

The experimental trajectory consisted of a rectangle with dimensions 550 mm and 350 mm in x and y directions, respectively. Machine speed was set to 8000 mm/min. Figure 2 shows an overview of the experimental set-up. Rectangle vertices (V1, V2, ..., V5) will serve as control points for evaluating measurement error in terms of 3D coordinates.

Sampling frequency was set to $f_s = 100$ Hz. The dead-reckoning algorithm is the one presented in section 3. Its unique parameter was set to $\beta = 0.001386$, obtained using equation 3.

We highlight that, although the trajectory is rather bi-dimensional, all 6 DoF of the IMU are activated in the measurement.

Implementation of data-processing package

Next we present the results of the data processing for this measurement task, in which the additional processing techniques described in section 3 are applied in a step-wise manner. Figure 3 shows the raw IMU outputs.

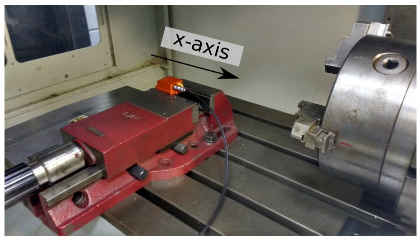

(a) IMU mounted on CNC platform.

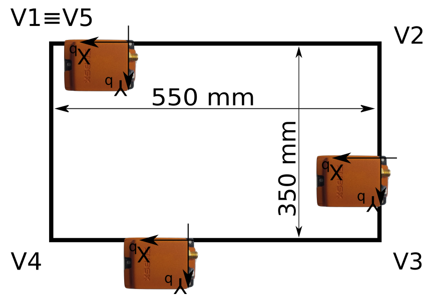

(b) Representation of the experimental trajectory. Motion starts at V1 and ends at V5.

Fig. 2: Experimental set-up.

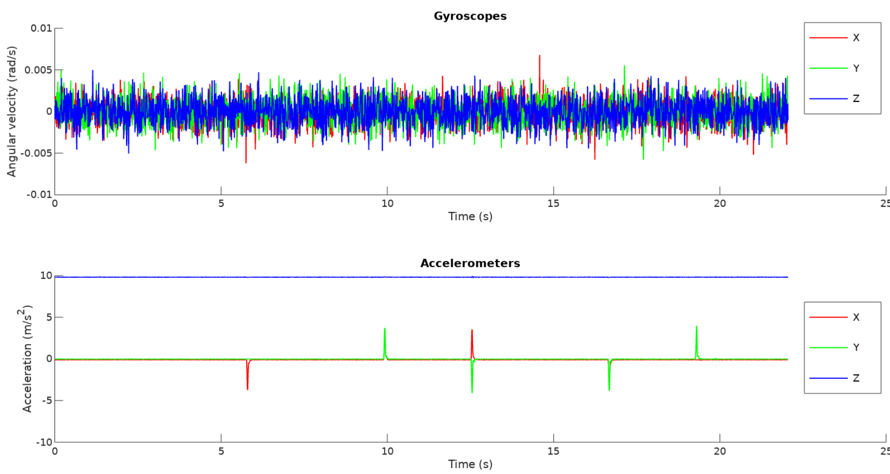

Fig. 3: IMU raw outputs from application example 1.

As could be expected, results of mere integration of measured inertial signals rapidly degenerate. Figure 4 shows the coordinates of the corresponding DR trajectory.

For the quantitative analysis, we define the *absolute positioning error* for each control point as the norm of the vector between the measured and the nominal point. Table 1 shows such errors in the current configuration (named **Configuration 0**).

The strategy for performing mathematical integration only during motion periods is now implemented over the same measurement data. Figure 5 shows the measured accelerations together with the identified periods of acceleration due to motion of the IMU.

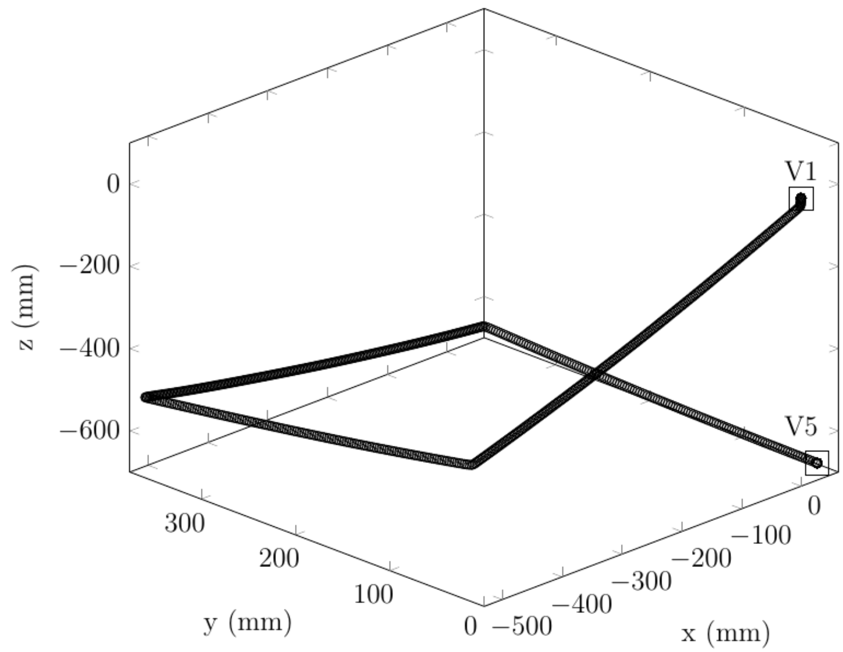

Fig. 4: DR result using no additional processing.

Configuration	V2	V3	V4	V5
0	386.97	540.14	675.17	700.83

Table 1: Absolute positioning errors (mm) of each control point using mere integration (Configuration 0).

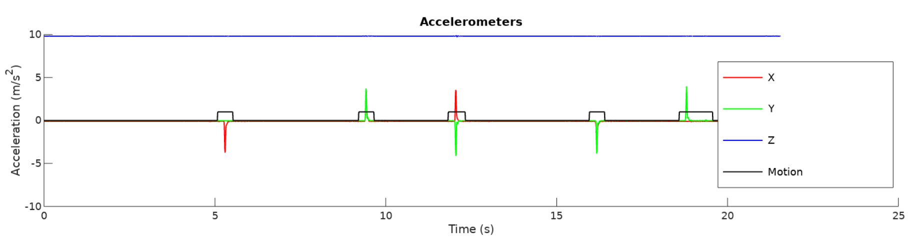

Fig. 5: Detection of motion periods.

Figure 6 shows the coordinates of the corresponding DR trajectory. It is noticeable that this implementation brought major improvements to the dead-reckoning results. Absolute positioning errors are shown in Table 2.

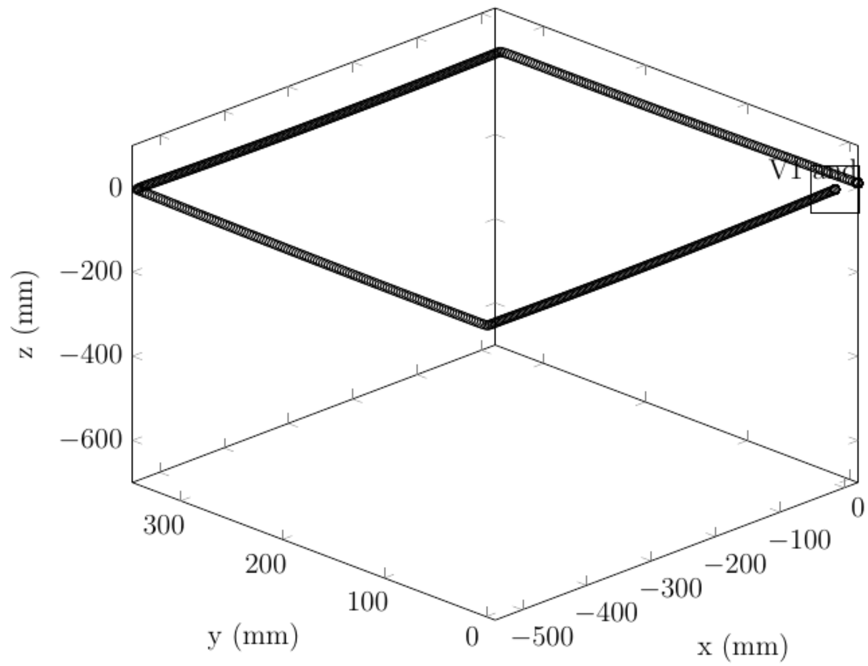

Fig. 6: DR result after implementation of the "motion detection" filter.

Configuration	V2	V3	V4	V5
0	386.97	540.14	675.17	700.83
1	32.17	44.30	44.49	25.74

Table 2: Absolute errors (mm) of each control point using motion detection filter (Configuration 1).

Next, results obtained from the multi-position calibration experiment were used to compensate for the residual fixed biases in each accelerometer (**Configuration 2**). For that, the average values of b_x, b_y and b_z were subtracted from the measured data of accelerometers in x, y, and z-axis, respectively. Positioning errors were reduced in a few millimeters.

Finally, **Configuration 3** includes the adaptive gain (β) strategy and the application of a wavelet filter. The former is not expected to have any influence in this case, since there are no changes in orientation along the trajectory. The latter, a wavelet filter using *Daubechies* wavelet mother with $J = 5$, was applied over the whole dataset.

Again, there was observed a few millimeters reduction in the positioning error for the various control points under this configuration. Table 3 shows the absolute positioning errors for all control points under each data-processing configuration. Figure 7 shows the same data in a visual fashion.

Configuration	V2	V3	V4	V5
0	386.97	540.14	675.17	700.83
1	32.17	44.30	44.49	25.74
2	30.96	43.74	44.41	23.22
3	30.63	42.61	35.94	10.76

Table 3: Absolute errors (mm) of each control point using motion detection filter (configuration 3).

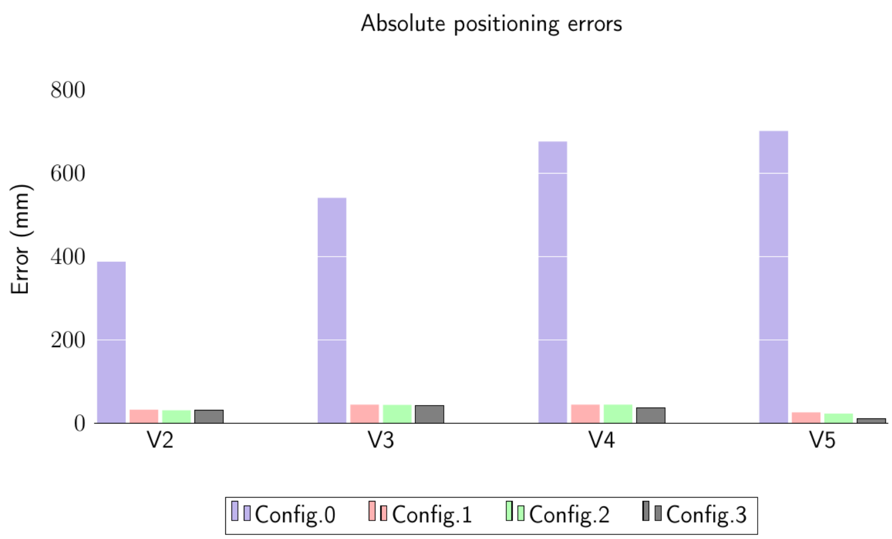

Fig. 7: Absolute positioning errors for points V2, V3 V4 and V5 using different configurations of the DR algorithm.

Figure 8 shows the dead-reckoning result after the implementation of the complete package of additional processing techniques. In brief, it can be seen that the adopted data-processing strategy had a positive effect on the dead-reckoning performance, yielding coherent measurement results. Greater contribution clearly comes from the motion detection strategy for this case.

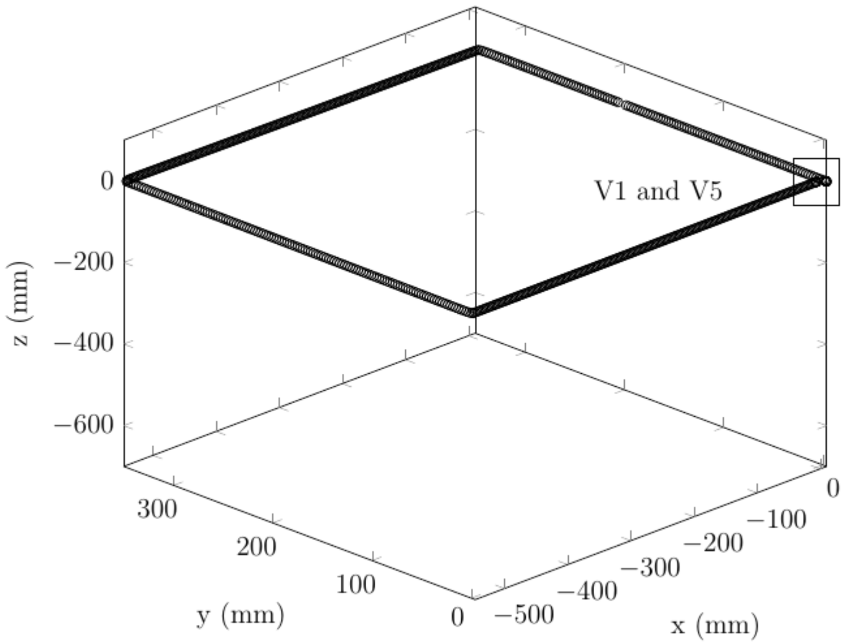

Fig. 8: DR result after implementation of the complete data processing package (Configuration 3).

4.2 Application example 2

The experimental data used in this example consists of an excerpt of a trajectory from the open-access dataset, dubbed "BROAD" — Berlin Robust Orientation Estimation Assessment Dataset, from [15]. The inertial sensor is the commercially available *myon aktos-t* IMU. Data-processing algorithms are the same as in application example 1.

Trajectory was generated by hand motion of the IMU, in volume of approximately (40 x 100 x 500) mm^3. Figure 9 shows the coordinates from ground-truth measurements and dead-reckoning results (already using configuration 3 of the data processing algorithm). Selected points (P1, P2 and P3) for analysis of the results are also highlighted in the figure.

Information of fixed bias values is not available in this case, and neither is the possibility of running a multi-position calibration experiment. In such situations, residual fixed biases of accelerometers will remain indistinguishably combined with the measured signals, which in turn will cause a corresponding decrease in the DR performance.

The absolute positioning errors of control points P1, P2 and P3 using different configurations of the data-processing package are shown in Table 4 and in

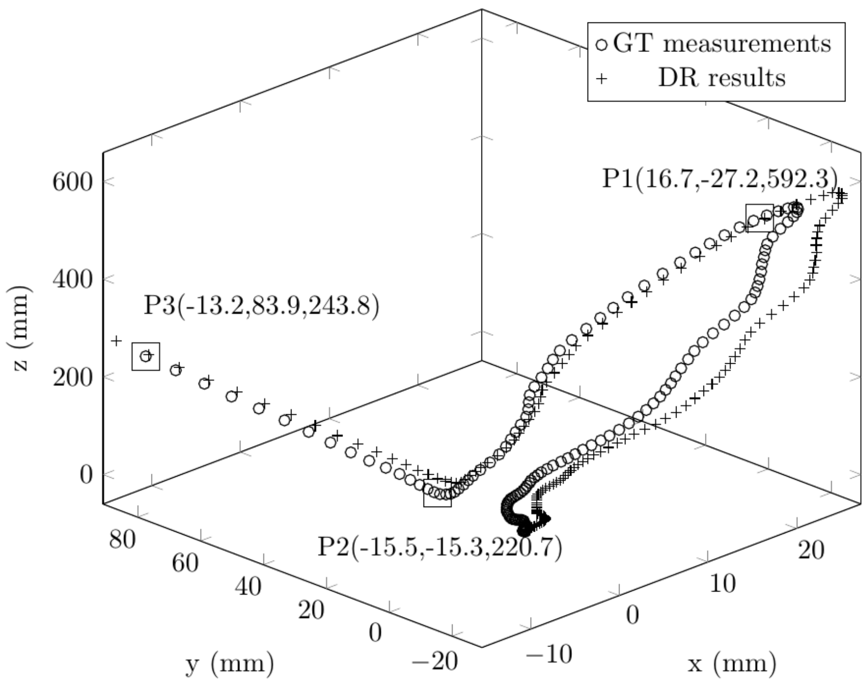

Fig. 9: DR result after implementation of the complete data processing package (Configuration 3).

Figure 10. Configuration 1 is not applicable, since residual fixed bias compensation(accelerometers) was not possible.

Configuration	P1	P2	P3
0	3247.7	3360.4	3404.2
2	16.94	32.13	60.06
3	10.53	15.99	78.13

Table 4: Absolute errors (mm) of each control point using different configurations of the data-processing package for application example 2.

Beneficial effects of the data-processing package can be observed also in this case. However, there is an exception in point P3, whose error grew from Config.2 to Config.3; reasons for this are not elucidated, but one possibility is that it may lie on the uncompensated accelerometers' biases.

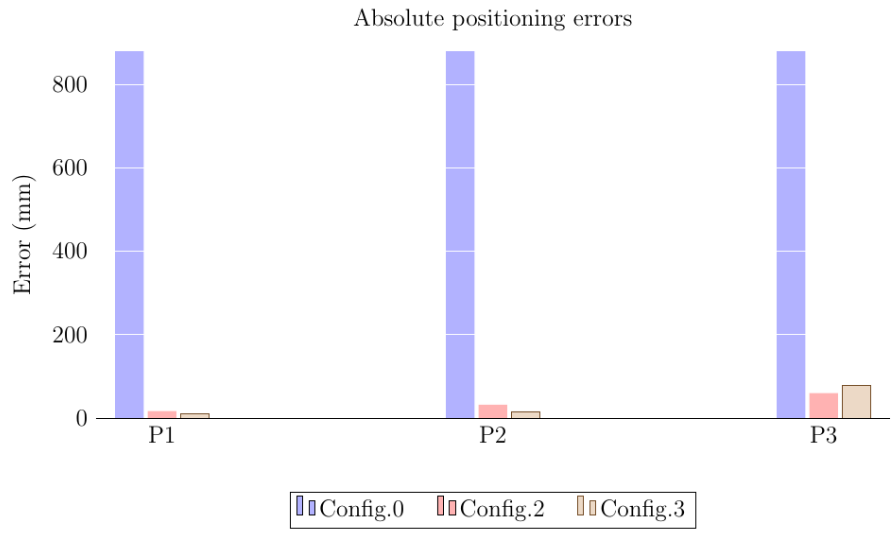

Fig. 10: Absolute positioning errors for points V2, V3 V4 and V5 using different configurations of the DR algorithm.

5 Conclusions

A DR algorithm has been presented, including a minimal data-processing package, based on a deep literature review and confirmed by experience gained through experimentation. This package has shown to bring significant benefits to the DR performance without the cost of highly specific manipulation of data. The use of 6 DoF IMU (i.e. only accelerometers and gyroscopes) limits the performance of orientation calculations, but has the advantage of not suffering with electromagnetic fields interference, wich is a common difficulty, specially in indoor environments. The general character of the processing package makes it likely to work well in a diversity of measurement tasks, as has been evidenced by the two application examples. Thus, it may serve as a starting point for other investigations on this subject. The organized overview of error sources affecting the measurement result of position, as well as the clarification of some relevant (and often misused) terms will contribute to further investigations on this matter, for instance, in the development of measurement uncertainty models. We believe this work lays relevant foundations for further studies regarding the measurement of position and orientation through dead-reckoning using six-degree-of-freedom MEMS-type IMUs.

Bibliography

[1] Jacques Georgy. Aboelmagd Noureldin, Tashfeen B. Karamat. *Fundamentals of Inertial Navigation, Satellite-based Positioning and their Integration*. Springer-Verlag Berlin Heidelberg, 2013.

[2] Juan Carlos Alvarez, Diego Álvarez, and Antonio M. López. Accelerometry-based distance estimation for ambulatory human motion analysis. *Sensors*, 18(12), 2018.

[3] Leslie Barreda Pupo. *Characterization of errors and noises in MEMS inertial sensors using Allan variance method*. Master of science thesis, Universitat Politecnica de Catalunya, 2016.

[4] Martin Brossard, Axel Barrau, and Silvère Bonnabel. AI-IMU Dead-Reckoning. *arXiv*, apr 2019.

[5] Marco Caruso, Angelo Maria Sabatini, Daniel Laidig, Thomas Seel, Marco Knaflitz, Ugo Della Croce, and Andrea Cereatti. Analysis of the accuracy of ten sensor fusion algorithms for orientation estimation using inertial and magnetic sensing under optimal conditions: a single outfit for every season does not work. *Sensors*, 21(2543):1–26, 2021.

[6] Changhao Chen, Xiaoxuan Lu, Andrew Markham, and Niki Trigoni. Ionet: Learning to cure the curse of drift in inertial odometry, 2018.

[7] R. Cohen. Signal denoising using wavelets project report. 2012.

[8] N. El-Sheimy, S. Nassar, and A. Noureldin. Wavelet de-noising for imu alignment. *IEEE Aerospace and Electronic Systems Magazine*, 19(10):32–39, 2004.

[9] IEEE. Ieee standard specification format guide and test procedure for single-axis interferometric fiber optic gyros. *IEEE Std 952-1997*, pages 1–84, 1998.

[10] IEEE. Ieee standard for inertial sensor terminology. *IEEE Std 528-2001*, pages 1–26, 2001.

[11] Kshitij Jerath, Sean Brennan, and Constantino Lagoa. Bridging the gap between sensor noise modeling and sensor characterization. *Measurement*, (September), 2017.

[12] Won-Yeol Kim, Hong-Il Seo, and Dong-Hoan Seo. Nine-axis imu-based extended inertial odometry neural network. *Expert Systems with Applications*, 178:115075, 2021.

[13] Manon Kok, Jeroen D. Hol, and Thomas B. Schön. Using inertial sensors for position and orientation estimation. *Foundations and Trends® in Signal Processing*, 11(1-2):1–153, 2017.

[14] Manon Kok and Thomas B. Schön. A Fast and Robust Algorithm for Orientation Estimation Using Inertial Sensors. *IEEE Signal Processing Letters*, 26(11):1673–1677, 2019.

[15] Daniel Laidig, Marco Caruso, Andrea Cereatti, and Thomas Seel. BROAD—A Benchmark for Robust Inertial Orientation Estimation. *Data*, 6(7):72, jun 2021.

[16] Jianwei Liu, Xixiang Liu, Wenqiang Yang, and Shuguo Pan. Investigating the survey instrument for the underground pipeline with inertial sensor and dead reckoning method. *Review of Scientific Instruments*, 92(2):2021, 2021.

[17] Wenxin Liu, David Caruso, Eddy Ilg, Jing Dong, Anastasios I. Mourikis, Kostas Daniilidis, Vijay Kumar, and Jakob Engel. TLIO: Tight Learned Inertial Odometry. *IEEE Robotics and Automation Letters*, 5(4):5653–5660, oct 2020.

[18] Sebastian O. H. Madgwick, Andrew J. L. Harrison, and Ravi Vaidyanathan. Estimation of imu and marg orientation using a gradient descent algorithm. In *2011 IEEE International Conference on Rehabilitation Robotics*, pages 1–7, 2011.

[19] Sebastian O. H. Madgwick, Samuel Wilson, Ruth Turk, Jane Burridge, Christos Kapatos, and Ravi Vaidyanathan. An extended complementary filter for full-body marg orientation estimation. *IEEE/ASME Transactions on Mechatronics*, 25(4):2054–2064, 2020.

[20] Milad Nazarahari and Hossein Rouhani. 40 years of sensor fusion for orientation tracking via magnetic and inertial measurement units: Methods, lessons learned, and future challenges. *Information Fusion*, 68(November 2020):67–84, 2021.

[21] Pedro Neto, J Norberto Pires, and Anónio Paulo Moreira. 3-D Position Estimation from Inertial Sensing : Minimizing the Error from the Process of Double Integration of Accelerations. In *Industrial Electronics Society, IECON 2013 - 39th Annual Conference of the IEEE*, pages 4024–4029, Vienna, 2013. IEEE.

[22] Cigdem POLAT and Mehmet Siraç ÖZERDEM. Introduction to Wavelets and their applications in signal denoising. *Bitlis Eren University Journal of Science and Technology*, 8(1):1–10, 2018.

[23] Robert H. Rogne, Torleiv H. Bryne, Thor I. Fossen, and Tor A. Johansen. On the usage of low-cost mems sensors, strapdown inertial navigation, and nonlinear estimation techniques in dynamic positioning. *IEEE Journal of Oceanic Engineering*, 46(1):24–39, 2021.

[24] Thomas Seel, Manon Kok, and Ryan S. McGinnis. Inertial sensors—applications and challenges in a nutshell. *Sensors*, 20(21), 2020.

[25] Sarra Smaiah, Rabah Sadoun, Abdelhafid Elouardi, Bruno Larnaudie, Samir Bouaziz, Abderahmane Boubezoul, Bastien Vincke, and Stéphane Espié. A practical approach for high precision reconstruction of a motorcycle trajectory using a low-cost multi-sensor system. *Sensors*, 18(7), 2018.

[26] David Tedaldi, Alberto Pretto, and Emanuele Menegatti. A robust and easy to implement method for imu calibration without external equipments. In *2014 IEEE International Conference on Robotics and Automation (ICRA)*, pages 3042–3049, 2014.

[27] Y K Thong, M S Woolfson, J A Crowe, B R Hayes-Gill, and R E Challis. Dependence of inertial measurements of distance on accelerometer noise. *Measurement Science and Technology*, 13(8):1163–1172, jul 2002.

[28] Daniel Weber, Clemens Gühmann, and Thomas Seel. Neural networks versus conventional filters for inertial-sensor-based attitude estimation. In *2020*

IEEE 23rd International Conference on Information Fusion (FUSION), pages 1–8, 2020.

[29] Samuel Wilson, Henry Eberle, Yoshikatsu Hayashi, Sebastian O.H. Madgwick, Alison McGregor, Xingjian Jing, and Ravi Vaidyanathan. Formulation of a new gradient descent marg orientation algorithm: Case study on robot teleoperation. *Mechanical Systems and Signal Processing*, 130:183–200, 2019.

[30] Li Xing, Xiaowei Tu, and Zhi Chen. Foot-mounted pedestrian navigation method by comparing adr and modified zupt based on mems imu array. *Sensors*, 20(13), 2020.

[31] Hang Yan, Qi Shan, and Yasutaka Furukawa. RIDI: robust IMU double integration. *Lecture Notes in Computer Science (including subseries Lecture Notes in Artificial Intelligence and Lecture Notes in Bioinformatics)*, 11217 LNCS:641–656, 2018.

[32] Tae Suk Yoo, Sung Kyung Hong, Hyok Min Yoon, and Sungsu Park. Gain-scheduled complementary filter design for a mems based attitude and heading reference system. *Sensors*, 11(4):3816–3830, 2011.

[33] WeiJie Zhang, Jun Xiao, and YuMing Zhang. Navigation of welding torch for arc welding process. In *IFAC Proceedings Volumes (IFAC-PapersOnline)*, volume 19, pages 7158–7163. IFAC, 2014.

[34] Ruoyu Zhi. *A Drift Eliminated Attitude & Position Estimation Algorithm In 3D*. Master of science, University of Vermont, 2016.